A Hierarchical Statistical Modeling Approach for the Unsupervised 3-D Biplanar Reconstruction of the Scoliotic Spine

Said Benameur*, Max Mignotte, Hubert Labelle, and Jacques A. De Guise

***Abstract*—This paper presents a new and accurate three-dimensional (3-D) reconstruction technique for the scoliotic spine from a pair of planar and conventional (postero-anterior with normal incidence and lateral) calibrated radiographic images. The proposed model uses *a priori* hierarchical global knowledge, both on the geometric structure of the whole spine and of each vertebra. More precisely, it relies on the specification of two 3-D statistical templates. The first, a rough geometric template on which rigid admissible deformations are defined, is used to ensure a crude registration of the whole spine. An accurate 3-D reconstruction is then performed for each vertebra by a second template on which nonlinear admissible global, as well as local deformations, are defined. Global deformations are modeled using a statistical modal analysis of the pathological deformations observed on a representative scoliotic vertebra population. Local deformations are represented by a first-order Markov process. This unsupervised coarse-to-fine 3-D reconstruction procedure leads to two separate minimization procedures efficiently solved in our application with evolutionary stochastic optimization algorithms. In this context, we compare the results obtained with a classical genetic algorithm (GA) and a recent Exploration Selection (ES) technique. This latter optimization method with the proposed 3-D reconstruction model, is tested on several pairs of biplanar radiographic images with scoliotic deformities. The experiments reported in this paper demonstrate that the discussed method is comparable in terms of accuracy with the classical computed-tomography-scan technique while being unsupervised and while requiring only two radiographic images and a lower amount of radiation for the patient.**

Manuscript received April 5, 2004; revised April 17, 2005. This work was supported in part by the Natural Sciences and Engineering Research Council of Canada under Project 107998-99, in part by the Canadian Foundation for Innovation, in part by Valorization Recherche Québec under Project 2200-003, and in part by the Biospace Company, Paris, France. *Asterisk indicates corresponding author.*

*S. Benameur is with the Imagery and Orthopedics Research Laboratory, Research Center, the University of Montreal Hospital Center (CRCHUM), Montreal, QC H2L 4M1, Canada. He is also with the Computer Vision and Geometric Modeling Laboratory, Computer Science and Operations Research Department, University of Montreal, Montreal, QC H2L 2W5, Canada (e-mail: benameus@iro.umontreal.ca).

M. Mignotte is with the Imagery and Orthopedics Research Laboratory, Research Center of the University of Montreal Hospital Center (CRCHUM), Montreal, QC H2L 4M1, Canada. He is also with the Computer Vision and Geometric Modeling Laboratory, Computer Science and Operations Research Department, University of Montreal, Montreal, QC H2L 2W5, Canada (e-mail: benameus@iro.umontreal.ca).

H. Labelle is with the 3-D Scoliosis Computational Laboratory, Research Center of Sainte-Justine Hospital, Montreal, QC H3T 1C5, Canada.

J. A. De Guise is with the Imagery and Orthopedics Research Laboratory, Research Center of the University of Montreal Hospital Center (CRCHUM), Montreal, QC H2L 4M1, Canada. He is also with the Automated Production Department of the École de technologie supérieure of Montreal, Montreal, QC H3C 1K3, Canada.

Digital Object Identifier 10.1109/TBME.2005.857665

***Index Terms*—Biplanar radiographies, energy function minimization, hierarchical statistical modeling, medical imaging, scoliosis, shape model, stochastic optimization, 3-D reconstruction model, 3-D/2-D registration.**

I. Introduction

In the past few years, there has been a great deal of research in reconstructing three-dimensional (3-D) shapes of anatomical structures from radiographic images. In medical imagery, this 3-D reconstruction problem remains a necessary step to obtain qualitative information, such as the detection of pathological deformations, as well as for quantitative measurements needed for surgical planning and follow-up evaluation. In this paper, we are concerned with computer vision methods for 3-D reconstruction of the scoliotic spine, from two X-ray radiographic images.

Scoliosis is a complex 3-D deformity of the natural curve of the spinal column, including rotations and vertebral deformations. The classical evaluation obtained by the spinal projections on the two-dimensional (2-D) radiographic planar images does not give a full and accurate interpretation of scoliotic deformities [1]. To analyze the 3-D characteristics of these deformations, several 3-D reconstruction methods have been developed. Among these methods, the 3-D reconstruction methods of tomodensitometric imagery modalities (e.g., computerized tomography [2], [3], or magnetic resonance [4], [5]) provide accurate 3-D information of the human anatomy or 4D information including time as one more degree of freedom. However, few hospitals can afford a magnetic resonance system, it is time-consuming, and the presence of nonferromagnetic metallic implants, once surgery has been performed, produces artifacts and creates suboptimal images. Tomodensitometric imagery systems have also another drawback, the high level of X-ray dose required to provide full 3-D data or large bone structures as the spine make them less functional. Also, these medical imaging techniques require that the patient be in a lying position, which is incompatible with many diagnostic protocols evaluating scoliosis.

For these abovementioned reasons, a 3-D reconstruction method of shapes using a limited number of X-ray radiographic projections and, thus ensuring a lower amount of radiation for the patient, is really interesting. Surprisingly, this problem has not been widely studied in the statistical framework, and few references exist in the computer vision and medical imagery

literature [6]–[8]. Among the proposed algorithmic techniques, we can cite the 3-D reconstruction method from silhouettes, proposed by Martin and Aggarwal in [9]. Their method allows to reconstruct polygonal 3-D objects by back-projecting the silhouettes. A method for extracting 3-D geometry of bones from two orthogonal X-ray radiographic projections is also proposed by Caponetti and Fanelli in [10]. The initial estimation of the 3-D bone structure, produced by back-projecting profile points, is then refined by using a B-spline interpolation. In [11], Benjamin generates surface information using common points, present in different projections, and the tracks between the points, extracted from about ten projection images.

Due to the ill-posed nature of this reconstruction problem, a right and accurate estimation of the 3-D geometrical structure of the shape cannot be found without constraints. In this way, methods using simple *a priori* knowledge on the geometrical structure of the object to be reconstructed and, thus, expressed as the solution of a regularized inverse problem, have been proposed. Terzopoulos *et al.* propose in [12] a method allowing to recover the 3-D shape from the 2-D profiles of an object using, as geometric prior constraint, a deformable tube coupled to a deformable spine. The deformation is controlled by physically based internal and external forces. Bardinet *et al.* present in [13] a method that consists in matching a parametric deformable model to unstructured 3-D data. More precisely, a super-quadric model is fitted to a given point set, and the generated super-quadric model is deformed locally using free-form deformations. In [14], Nikkhade *et al.* present 3-D reconstruction method of femurs from two orthogonal X-ray radiographic projections. They separate the femur into three subparts; each of them assumed to be round. They fit cubic parametric surface patches to the subparts and then assemble them to a complete model. Kita develops in [15] a method allowing to analyze X-ray radiographic projections of the stomach using a deformable 3-D model. Their *a priori* model is a tube which is first initialized using only one projection. Afterward, the model is deformed using the other projections. Nevertheless, in these methods, the geometric *a priori* constraint does not model the set of admissible deformation (or in the case of scoliosis, the pathological variability) of the anatomical structure to be reconstructed. Consequently, the 3-D reconstructed shape estimation does not necessarily correspond to the reality.

In order to rightly constrain the ill-posed nature of this problem, a solution consists in supervising the 3-D reconstruction technique. In this sense, a 3-D multiplanar radiography reconstruction method using a direct linear transformation (DLT) [16] is presented by Dansereau and Stokes in [17]. They rely on manual stereo-digitization of six anatomical landmarks (on each X-ray radiographic image) of the vertebrae to produce 3-D coordinates. Adding the kriging technique using the 3-D reconstructed points as control points yields good visualization of the vertebral geometry [18]. There is a need for more landmarks to obtain a better description of all the vertebrae. In the same way, a nonstereo corresponding points technique is also described by Mitton *et al.* in [19] to improve the accuracy of the 3-D reconstruction by identifying more anatomical landmarks on the X-ray projections. This method is then based on deformation of an elastic deformable mesh that respects stereo corresponding and nonstereo corresponding points available in different X-ray radiographic projections. In addition to the supervision, the methods proposed by Dansereau *et al.*, Mitton *et al.* and Delorme *et al.* are limited due to the inherent inaccuracy produced in identifying anatomical landmarks (leading to reconstruction errors). Marcil *et al.* have studied in [20] an effect of the displacement of the patient between the X-ray exposures in the 3-D stereoradiographic of scoliotic spines and rib cages. Besides, they do not exploit all the information contained in the two X-ray radiographic projections (e.g., the contours of each vertebra) or the statistical knowledge of the possible deformation of the object to be reconstructed. Lavallée *et al.* [21] describe an algorithm which minimizes the 3-D distances between the rays (corresponding to the points on the contour) and the closest point on the surface of the object. A 3-D distance map is precomputed that stores the distance from any point in the neighborhood of the object to the closest point on the surface. Lavallée developed an octree-spline technique to speed up the construction of the distance map, which otherwise would be prohibitively slow. The primary disadvantage of octree-spline is the time it takes to build the octree. In addition, the octree-spline representation of a data set is highly dependent on the initial position and orientation of the data; two data sets that differ only by a small translation or rotation may have substantially different octree-spline representations. The iterative closest point (ICP) [22] starts with two meshes and an initial estimation for their relative rigid-body transformation, and iteratively refines the transformation by repeatedly generating pairs of the closest points on the meshes and minimizing an error metric. ICP has a disadvantage that a correct registration is not guaranteed. Since it is a deterministic minimization method, the algorithm is likely to fall into a local minimum. Consequently, combining octree-spline with ICP algorithm for 3-D reconstruction of scoliotic spine requires a good initial estimate of the position and orientation of each vertebra in a radiographic environment.

Methods using statistical *a priori* knowledge of the geometric shapes of the objects of interest lead to better constrain the reconstruction problem. In [23], Fleute and Lavallée propose a method allowing to reconstruct the 3-D geometry of the femur using a few orthogonal X-ray radiographic projections. They apply point distribution models (PDM) [24] to reconstruct a geometric prior model representing mean shapes and containing the typical deformation modes in statistical sense. Thereafter, they deform the model nonrigidly, according to the rays back-projected from the contour points of the projections taken from a patient. Benameur *et al.* propose in [25] a 3-D statistical reconstruction method, for each individual vertebra, using a pair of planar and conventional (postero-anterior with normal incidence and lateral) radiographic images for a patient in a standing position, and a prior global knowledge of the geometric structure of each vertebra. The method consists of fitting the projections of this deformable template with the preliminary segmented contours of the corresponding vertebra on the two X-ray radiographic projections. Nevertheless the above-mentioned technique remains widely supervised and requires the knowledge of the position of six anatomical points (namely, the center of the superior and inferior end-plates, the

upper and lower extremities of both pedicles) to initialize 3-D reconstruction process of each vertebra of the spine.

To overcome this problem of supervision and improve the 3-D reconstruction and the optimizer related to the energy-based model presented in [25], we propose in this paper a 3-D statistical reconstruction method based on the likelihood introduced in [25] but using hierarchical global *a priori* knowledge on the geometric structure of both the whole spine and each vertebra. Hierarchical statistical models have been applied in a fusion of multiresolution image data [26], segmentation [27], [28], restoration [29] and in active shape models using the wavelet transform [30]. Bernard *et al.* introduce in [28] a hierarchical strategy for segmenting cervical vertebrae. This hierarchical scheme is comprised of two levels; shape and appearance models. Appearance model describes individual structures and forms the lower level, while the topological or shape model, describing the organization of anatomical structures, forms the upper level, respectively. This method is not applied to the 3-D reconstruction problem (using two or several X-ray views) but only to the segmentation of cervical vertebrae using a single X-ray view.

To our knowledge, no hierarchical statistical model for 3-D reconstruction methods have been described in the literature. More precisely, the hierarchical model we propose relies on the specification of two 3-D templates. The first, a rough and cubic approximation geometric template on which rigid admissible deformations are defined, is used to fit its (postero-anterior and lateral) projections with the preliminary segmented contours of each vertebra body of the spine on the two calibrated radiographic views. It ensures crude registration of the whole spine and gives a rough position and orientation of each vertebra. Three-dimensional reconstruction is then refined by a second template which takes into account *a priori* global knowledge on the geometric structure of each vertebra. This geometric knowledge is efficiently captured by a statistical deformable template integrating a set of admissible deformations, expressed by the first modes of variation in Karhunen–Loeve (KL) expansion, of the pathological deformations observed on a representative scoliotic vertebra population. A global deformation applied to the model. A local deformation process, which assumed to follow a first-order Markovian process, is then used to refine the model. This unsupervised coarse-to-fine 3-D reconstruction procedure leads to two optimization problems related to two (coarse and fine) energy-based models. These two optimization problems are efficiently solved in our application with a recent stochastic optimization technique based on an Exploration Selection procedure. Finally, we propose a complete validation of the proposed reconstruction technique.

This paper is organized as follows. Section II presents the hierarchical prior model used in our coarse-to-fine reconstruction method. Section III describes silhouette extraction of the 3-D model. Section IV briefly recalls the likelihood model and the 3-D/2-D registration strategy introduced in [25]. Section V presents energy function minimization related to the coarse-to-fine registrations and the stochastic optimization procedure used to estimate optimal reconstruction. Section VI presents the validation protocol of 3-D reconstruction method. In Section VII, we show some 3-D reconstruction results and validate the proposed model.

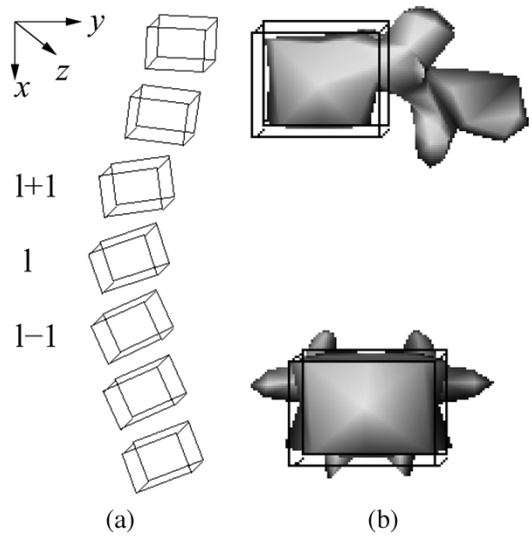

Fig. 1. Crude prior model of the spine. (a) Deformable model of the whole spine and (b) cubic template representation associated with each vertebra.

II. Coarse-to-Fine Prior Model

A. Crude Prior Model of the Spine

To ensure crude registration of the whole spine and to estimate a rough position t, scale k and orientation α of each vertebra, we first consider a crude *a priori* geometric model for the whole spine [31] (justified by the fact that each vertebral body is nearly parallelepiped in shape and of similar size).

This model relies on a set of cubic templates, roughly representing each vertebral body and stacked on top of one another to form the spinal column (e.g., Fig. 1). Each cubic template (defined by a set of control point vectors of the cubic representation) associated with each vertebral level has its scale, orientation and position constrained within a restricted domain whose center is given by knowledge of the (previously) estimated parameters of the cubic template which is located below.

We manually identify the center of the superior and inferior end-plate of the lowest vertebra of the spine on the two radiographic views. User interaction is limited to simply placing these points on the two radiographic images (thanks to a graphical user interface). The 3-D coordinates of these landmarks are obtained by DLT [16]; the corresponding points on the cubic template being known. We estimate the rigid transformation allowing us to pass from the set of center of the superior and inferior end-plate of cubic template to the set of the reconstructed center of the superior and inferior end-plate of the lowest vertebra of the spine. Then, we apply this rigid transformation to all points of the cubic template. Once this is done, we optimize the rigid transformation, which enables us to readjust the two sets of center of the superior and inferior end-plate. We re-apply the rigid deformation to all points of the cubic template. This procedure is repeated until the difference in variation of error between two successive stages is lower than a given threshold.

The coordinate system used for the following equation is mentioned on Fig. 1. For example, if the registration of the whole crude spine is made from bottom to top, then the position

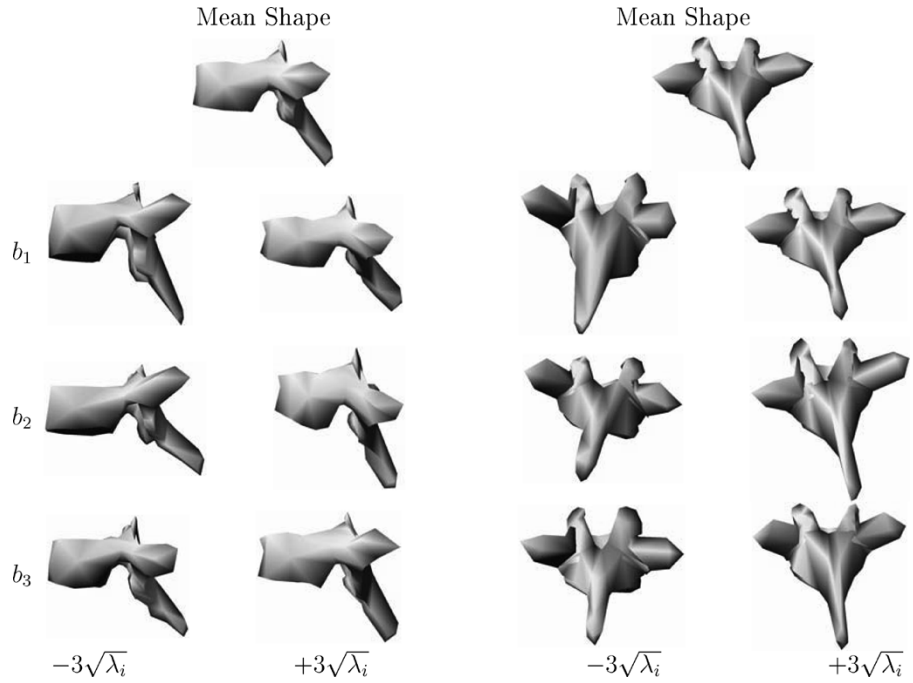

Fig. 2. Fine prior model of each vertebra. Two deformed shapes obtained by applying three standard deviations of the first three deformation modes to the mean shape of $T8$ vertebra and from the sagital and coronal views.

$t^l = (t^l_x, t^l_y, t^l_z)$, scale vector $k^l = (k^l_x, k^l_y, k^l_z)$ and orientation $\alpha^l = (\alpha^l_x, \alpha^l_y, \alpha^l_z)$ at (vertebral) level l, given the rough parameter estimation of vertebra below the level l (i.e., $l-1$), are restrained within the domain defined by

$$\begin{aligned} t^{l-1}_x + k^{l-1}_x \le t^l_x \le t^{l-1}_x + k^{l-1}_x + \Delta t^l_x \\ t^{l-1}_y - \Delta t^l_y \le t^l_y \le t^{l-1}_y + \Delta t^l_y \\ t^{l-1}_z - \Delta t^l_z \le t^l_z \le t^{l-1}_z + \Delta t^l_z \\ k^{l-1} - \Delta k^l \le k^l \le k^{l-1} + \Delta k^l \\ \alpha^{l-1} - \Delta\alpha^l \le \alpha^l \le \alpha^{l-1} + \Delta\alpha^l \end{aligned}$$

where α is the rotation vector (ensuring the rotation in x, y or z axes). Δt_x, Δt_y, Δt_z, Δk and $\Delta\alpha$ are given by statistical knowledge on the scoliotic deformation of the spine [32], [33]. We take for the range of $\Delta k = (\Delta k_x, \Delta k_y, \Delta k_z)$, $\Delta\alpha = (\Delta\alpha_x, \Delta\alpha_y, \Delta\alpha_z)$, and $\Delta t = (\Delta t_x, \Delta t_y, \Delta t_z)$

$$\begin{aligned} (-3,-3,-3) \le \Delta k \le (+3,+3,+3) \\ (-5^\circ,-5^\circ,-5^\circ) \le \Delta\alpha \le (+5^\circ,+5^\circ,+5^\circ) \\ (-5,-5,-5) \le \Delta t \le (+5,+5,+5). \end{aligned}$$

A global configuration of the deformable spine model is, thus, described by 9 rigid transformation parameters for each cubic template associated with each vertebral level.

B. Fine Prior Model of Each Vertebra

Our *a priori* knowledge model relies also on the description of each vertebra by a 3-D deformable template (i.e., a vector $s \in R^{3n}$ of n control points) which incorporates statistical knowledge about its geometrical structure and its pathological variability. The deformations of this template are expressed by the first modes of variation in KL expansion of pathological deformations observed on a representative training scoliotic vertebra population [25]. This can be done by using principal component analysis (PCA), i.e., by computing the covariance matrix C of shapes $\{s_i\}$. The main deformation modes of the template model s are then described by the eigenvectors ϕ of C, with the largest eigenvalues λ (e.g., Fig. 2).

C. Deformable Template Representation

The shape s of each vertebra of our training database described in Section VII-A is represented as a template, that is a set of points or landmarks[1]

$$s = (p_1, p_2, \ldots, p_i, \ldots, p_n)^T$$

where $p_i = (x_i, y_i, z_i)^T$ are the Cartesian coordinates of each surface point.

Given a sample $s_1, \ldots, s_n$ of shapes with the same number of points, we resort to the procedure proposed in [35] to align this training set. We then apply the PCA to reduce the dimension to $m \ll 3n$. m is defined in such a way that it describes a certain proportion of possible variations. This gives us nonlinear deformations of the mean shape $\bar{s}$ and terminates the training phase.

[1]These landmarks are obtained by measuring specific anatomical landmarks on each vertebra specimen using a pointer of the electromagnetic device, thus creating a set of approximately 200 points depending on the level measured with regard to its particular geometry [34] (see Section VII-A). Different points were acquired in a specific order and recorded in this sequence. All vertebrae of same vertebral level have the same number of points, and the 3-D coordinates of points of each vertebra were recorded in a specific order. Each set of points was then re-localized in a local coordinate system.

1) Global Deformations: The globally deformed template is defined by

$$s = M(k, \boldsymbol{\alpha})[\overline{s} + \Phi b] + T \tag{1}$$

where the following hold.

- T and $M(k, \alpha)$ account for rigid deformations of the template, (T is a global translation vector, and $M(k, \alpha)$ performs a rotation (in the x, y or z axes) and a scaling by k). In our application the initial k, α and T for the fine model are given by the estimation of the k, α and T obtained by optimization of the crude model.
- $\Phi = (\phi_1, \ldots, \phi_m)$ is the matrix of the first m eigenvectors of C associated with the m largest eigenvalues and $\mathbf{b} = (b_1, \ldots, b_m)^T$ is a vector containing the weights for these m deformation modes.

A global configuration of the deformable vertebra template is, thus, described by $7 + m$ parameters corresponding to rigid transformations and m modal weights b_j. Due to the KL transform, the random variables b_i are independent and follow a normal law of a null mean and variance λ_i. Thus, the law of probability of s, the deformed template, can be written as [25]

$$P\left(s(\theta)\right) = \mathcal{U}(T, k, \alpha) \prod_{i=1}^{m} \frac{1}{\sqrt{2\lambda_i \pi}} \exp\left(-\frac{b_i^2}{2\lambda_i}\right) \tag{2}$$

where $\mathcal{U}$ denotes the uniform distribution with appropriate bounds for the 9 affine transformation parameters (including the scale factor).[2] This low parametric representation for each vertebra level, along with the crude parametric representation of the whole spinal column constitutes our global hierarchical *a priori* model that will be used to rightly constrain the ill-posed nature of our proposed coarse-to-fine 3-D reconstruction method.

By letting $E_p(s(\theta))$, the *a priori* energy term related to the prior distribution [see (3)], can be written as

$$E_p\left(s(\theta)\right) = \frac{1}{2} \sum_{i=1}^{m} \frac{b_i^2}{\lambda_i} \tag{3}$$

which is close to the Mahalonobis distance. This prior energy term penalizes the deviation of the deformed template from the mean shape (and not the affine transformations). This prior energy term will be used later in (9).

2) Local Deformations: In our application, the local deformation process allows to take into account firstly, the fact that our PCA does not model 100% of the scoliotic and natural biological deformations (between individuals) of our vertebra database, the first m deformation modes are chosen in order to get a reasonably low parametric representation model) and, secondly, the fact that our vertebra database could not be big or representative enough and consequently could not certainly contain all the possible scoliotic deformations (30 normal and 30 scoliotic for each vertebral level). Inspired by the work of Grenander and Keenan on stochastic pattern representation [36], a statistical local deformations process δ is now applied to the n control points or "landmarks" which approximate the geometrical shape of each vertebra.

These local deformations are modeled as local random perturbations of the shape and can be considered as a refinement of the global deformations applied to the deformed mean shape, since the main deformation modes have already been captured by the preliminary global statistical prior knowledge of each vertebra. The local deformation vector $\delta = (\delta_1, \delta_2, \ldots, \delta_n)^T$ with $\delta_i = (\delta_{x_i}, \delta_{y_i}, \delta_{z_i})$ is described by a first-order Gauss-Markov process defined on the graph corresponding to the n control points of the deformable template of each vertebra. If we represent these local deformations by local random translations (that are superimposed on the globally deformed shape), the complete (i.e., globally and locally) deformable model of each vertebra can be defined by

$$\hat{s} = M(k, \boldsymbol{\alpha})[\overline{s} + \Phi b] + T + \delta. \tag{4}$$

Assuming a first-order neighborhood structure on the graph associated to the n control points of the deformable template, the probability distribution of the random field δ can be written as

$$P(\delta) = \frac{1}{\zeta} \exp\left(-E_r(\delta)\right)$$

where ζ is a normalization constant, and $E_r(\delta)$ is the local deformation energy term which can be written as

$$E_r(\delta) = \frac{1}{2} \sum_{i=1}^{n} \left(\frac{1}{\mu_i^2} \sum_{j \in \mathcal{N}(i)} \|\delta_i - \delta_j\|^2 + \frac{1}{\nu_i^2} \|\delta_i\|^2 \right) \tag{5}$$

where $\mathcal{N}(i)$ is the set of first-order neighborhood of point i, μ_i^2, and ν_i^2 are the variance parameters of this local deformation model. μ_i^2 weighs the interactions between neighboring points. ν_i^2 control the amplitude of the local deformations compared to the globally deformed model. In our application, we consider $\mu_i = \mu$ and $\nu_i = \nu$, $\forall i$, since the different control points of our 3-D vertebra template are approximatively equally spaced. This local deformation energy term will be used later in (9).

III. Silhouette Extraction of the 3-D Model

The 3-D model of vertebrae is represented in the form of a triangulated mesh. Silhouette occurs when a triangle faces toward the projection source and a neighbor triangle across an edge faces away from the source. So for two triangles T_i and T_j with normals $\vec{n}_i$ and $\vec{n}_j$ and a view vector $\vec{v}$, a shared edge is a silhouette edge if

$$(\vec{n}_i \times \vec{v}) \cdot (\vec{n}_j \times \vec{v}) \leq 0$$

where "$\times$" and "$\cdot$" denote, respectively, the vector and scalar product.

On a surface, the silhouette edge of the vertebra shape are lines where the direction of projection is tangent to the surface. As in the case of a not-convex object, the silhouette edges can be hidden by other parts of the surface. We keep all the edges,

[2] An interesting alternative would have been to consider a Gaussian prior distribution for the scale factor, but this *a priori* assumption would have required, as a preliminary, estimate the parameters of this Normal law.

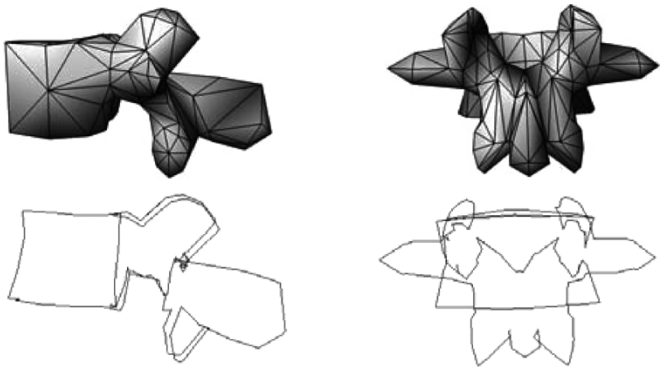

Fig. 3. Example of lateral and postero-anterior outlines from a 3-D model.

including those that are occluded. Let us recall that we use semi-transparent radiographic images [25]. Fig. 3 shows an example of silhouette from a 3-D model.

IV. Likelihood Model

As proposed in [25], the likelihood model is expressed by a measure of similarity between the external contour of the (postero-anterior and the lateral) projections of the 3-D deformed template and a directional edge potential field estimated on the two radiographic views. This likelihood energy term is defined by

$$E_l\left(s(\theta), I_{\mathrm{PA}}, I_{\mathrm{LAT}}\right) = -\frac{1}{n_{\mathrm{PA}}} \sum_{\Gamma_{\mathrm{PA}}} \Psi_{\mathrm{PA}}(x,y) - \frac{1}{n_{\mathrm{LAT}}} \sum_{\Gamma_{\mathrm{LAT}}} \Psi_{\mathrm{LAT}}(x,y) \quad (6)$$

where the summation of the first and second term of E_l is overall the n_{PA} and n_{LAT} points of the external contour of the, respectively, lateral (I_{LAT}) and postero-anterior (I_{PA}) perspective projections of the deformed template on the two precomputed edge potential fields of each radiographic image. The 2-D perspective projections of the 3-D deformed template, i.e., the lateral and postero-anterior outline is computed with the silhouette extraction algorithm.

To compute the edge potential field Ψ associated with each radiographic view, we first use a Canny edge detector with the unsupervised technique proposed in [37]. Then, Ψ is defined as in [38] by

$$\Psi(x,y) = \exp\left(-\frac{\sqrt{\xi_x^2 + \xi_y^2}}{\tau}\right) \left|\cos\left(\gamma(x,y)\right)\right| \quad (7)$$

where $\xi = (\xi_x, \xi_y)$ is the displacement to the nearest edge point in the image, and τ is a smoothing factor which controls the degree of smoothness of this potential field. $\gamma(x,y)$ is the angle between the tangent of the nearest edge and the tangent direction[3] of the contour at (x,y) (e.g., Fig. 4). This likelihood energy

[3]For each point (x,y) on the projected silhouette of the 3-D model, we have to calculate the nearest edge point (x',y') in the image. We then calculate the tangent vector of the silhouette at point (x,y) and its successor, the vector tangent of the nearest edge at point (x',y') (by a gradient estimation), and the angle between these two tangents. This definition requires that the projected silhouette agrees with the segmented contours in position and in the tangent direction.

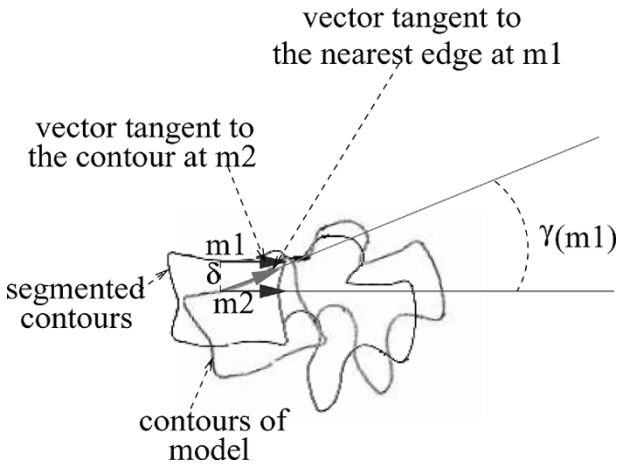

Fig. 4. Directional component used in the directional edge potential field $\Psi(x,y)$.

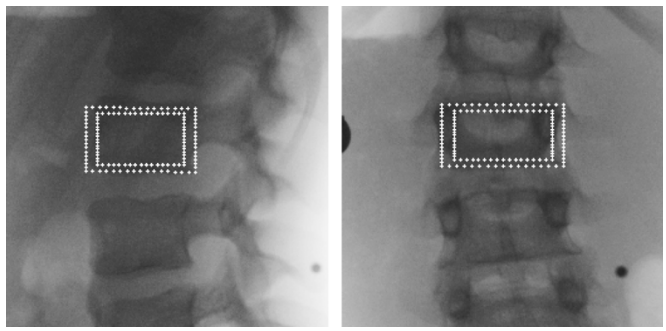

Fig. 5. The two projected contours of the shape of cube templates with scale k and a slightly larger scale $k+\epsilon$ on the corresponding vertebral body on postero-anterior and lateral views.

term, as expressed in (6), is exploited for the 3-D reconstruction of the fine prior model of each vertebra (see Section II-B). In order to ensure a good reconstruction of each cube template of the crude prior model of the spine (see Section II-A), which will be used to initialize this latter fine 3-D reconstruction, we propose to improve this likelihood measure with the following heuristic; let s_0 and s_1 denote the shape of one cube template with scale k and a slightly larger scale $k+\epsilon$, respectively. The considered likelihood energy term is expressed as

$$E_l\left(s(\theta), I_{\mathrm{PA}}, I_{\mathrm{LAT}}\right) = E_l\left(s_0(\theta), I_{\mathrm{PA}}, I_{\mathrm{LAT}}\right) - E_l\left(s_1(\theta), I_{\mathrm{PA}}, I_{\mathrm{LAT}}\right). \quad (8)$$

The better the correspondence between the (postero-anterior and lateral) projected contours of the inner cube template s_0 and the preliminary segmented contours of the two radiographic views (expressed by $E_l(s_0(\theta), I_{\mathrm{PA}}, I_{\mathrm{LAT}})$) and no correspondence between the projected contours of the outer cube template s_1 and the presegmented contour map $(E_l(s_1(\theta), I_{\mathrm{PA}}, I_{\mathrm{LAT}}))$, the closer this measure will be to the minimum. Experiments have shown that this heuristic allows to obtain a better matching when the crude registration is used on low resolution, low contrast and low signal-to-noise ratio radiographic images (e.g., Fig. 5).

V. Coarse-to-Fine Optimization Strategy

This unsupervised coarse-to-fine 3-D reconstruction procedure is stated as a double energy function minimization problems, namely

$$E\left(s(\theta),\delta\right) = E_l\left(s(\theta), I_{\mathrm{PA}}, I_{\mathrm{LAT}}\right) + \beta\left(E_p\left(s(\theta)\right) + E_r(\delta)\right) \tag{9}$$

where E_l is the likelihood energy term enforcing data closeness, $(E_p + E_r)$ is the prior energy term enforcing regularity in the Tikhonov sense. β is a factor allowing to control the balance between the two energy components and the rigidity of the deformable template.

The energy function to be minimized is complex with several local minima over the deformation parameter space. A global search is impossible due to the size of the configuration space. Let us also add that the quality of the reconstruction is closely related to the good estimation of the deformation parameters and consequently to the performance of the optimization procedure. In our application, we use the stochastic optimization algorithm recently proposed by François in [39]. We use this algorithm because the adjustment of all internal parameters does not depend on the function to be minimized. Moreover, the convergence is asymptotically ensured [39]. Let us add that this optimization algorithm is also especially well suited to minimize complex (i.e., nonconvex) energy functions [40]. We compare the performance of this algorithm, in Section VII, with a classical genetic algorithm (GA) [41].

A. Exploration/Selection Algorithm

The E/S algorithm belongs to the class of evolutionary algorithms. This class of algorithm has been successfully applied in diverse areas such as medical imaging [42] and localization of shapes [40] to minimize complex energy functions [40]. This success has initiated the development of various evolutionary algorithm variants and stimulated the theoretical research about convergence properties of these algorithms (see [43] for a good review of evolutionary algorithm in medical imagery).

The E/S algorithm can be summarized as follows (more details are given in [39]). Let F be a finite discrete subset of the Cartesian product of k compact intervals $[m_i, M_i]$, for $1 \leq i \leq k$, and $\theta = \{\theta_1, \ldots, \theta_n\}$ a set of n potential solutions randomly chosen. We define $\hat{\theta}$ as the optimal element θ_i of θ such that $E(s(\theta_j)) > E(s(\theta_i))$, for $1 \leq j < i$, and $E(s(\theta_j)) \geq E(s(\theta_i))$, for $1 < j \leq n$. We consider a graph G defined on F called the *exploration graph*. The exploration graph is assumed to be nonoriented and connected. We denote by $\mathcal{N}(a)$ the neighborhood of the element $a \in F$ in the graph G defined by $\{b \in F : \text{for some } j, |b_j - a_j| \leq r(M_j - m_j), b_i = a_i, i \neq j\}$ where r is a real number in the interval [0,1] called the radius of exploration.

Each solution of θ is regarded as an individual that attempts a random search on the exploration graph [39]. For $b \in F$, we fix a positive distribution a_b on $\mathcal{N}(b)$. The exploration process acts independently on each individual, and consists of choosing a random N according to the positive distribution. We replace θ_i by $\vartheta_i \in \mathcal{N}(\theta_i) \setminus \{\hat{\theta}\}$ according to a uniform distribution, for $i \leq N$ otherwise, we change θ_i by $\hat{\theta}$. This process is run until a fixed maximum number of iterations has been reached (see Algorithm. 1).

Algorithm 1: *E/S Optimization Algorithm*

E/S Algorithm

$E(.)$	A real-valued l-variable function, defined on F, to be minimized
F	A finite discrete subset of the Cartesian product $\Pi_{j=1}^{l}\{m_j, M_j\}$ of l compact intervals
n	The size of the population (greater than D)
r	A real number $\in [0,1]$ called the radius of exploration (with r greater than the ϵ machine)
$\mathcal{N}(a)$	The neighborhood of an element $a \in F$ defined by $\{b \in F :$ for some $j \in [1,l], \lvert b_j - a_j \rvert \leq r(M_j - m_j), b_i = a_i, i \neq j\}$
$D = l/r$	The diameter of the exploration graph endowed with the system of neighborhood $\{\mathcal{N}(a)\}_{a \in F}$
θ	$\theta = \{\theta_1, \ldots, \theta_n\}$, an element of F^n
$\hat{\theta} \in F$	$\hat{\theta} = \arg\min_{\theta_i \in \theta} E(\theta_i)$, i.e., the minimal point in θ with the lowest label
p	The probability of exploration
k	The iteration step

1. **Initialization**
   Random initialization of $\theta = \{\theta_1, \ldots, \theta_n\} \in F^n$ $k = 2$
2. **Exploration/Selection**
   repeat
   1) Compute $\hat{\theta}$; $\hat{\theta} = \arg\min_{\theta_i \in \theta} E(\theta_i)$
   2) Draw m according to the binomial law $b(n,p)$
   - For $i \leq m$, replace θ_i by $\vartheta_i \in \mathcal{N}(\theta_i) \setminus \{\hat{\theta}\}$ according to the uniform distribution (Exploration step)
   - For $i > m$, replace θ_i by $\hat{\theta}$ (Selection step)
   3 $k = k + 1$ and $p = k^{-1/D}$
   until *a criterion met*;

This optimization problem can be divided into three steps. The first step corresponds to crude reconstruction in which $E_p = 0$ and $E_r = 0$. In the second step, we refine the crude reconstruction by a second optimization step which takes into account a prior global knowledge on the geometric structure of each vertebral level, and which considers the local deformations as negligible ($\delta_i = 0, \forall i$). Finally, a last refinement of the reconstruction is performed by using local deformations. These steps are explained in more detail in Sections V-B, V-C, and V-D, respectively.

B. Crude Reconstruction

This energy-based model is first used for the registration of the whole spine with the set of cubic templates presented in

Section II-A and the likelihood measure presented in (8). In this crude reconstruction step, there is no prior energy term ($E_p = 0$ and $E_r = 0$) since we do not use nonlinear and local deformations. The ill-posed reconstruction problem is nevertheless constrained by the low parametric representation of the whole spine and the restricted search space defined for each cubic template (see Section II-A). After optimization, this crude registration allows to estimate the rough position $T = (T_x, T_y, T_z)$, scale k and orientation $\alpha = (\alpha_x, \alpha_y, \alpha_z)$ of each vertebra.

C. Fine Reconstruction With Global Deformations

This optimization problem is then used with the fine prior template of each vertebra (see Section II-B and the likelihood measure proposed in (6). Optimization is made within a range of values around the rigid parameters roughly estimated by the first crude reconstruction given in Section V-B. In this section, we consider the local deformations as negligible ($\delta_i = 0$, $\forall i$) and we have to estimate $\theta = (k, \alpha, T, b)$, i.e., $7+m$ parameters corresponding to rigid transformations and m modal weights b_j. For this fine reconstruction with global deformations, we take as scaling parameter k the mean value of the three scaling parameters k_x, k_y, and k_z obtained in crude reconstruction step.

D. Fine Reconstruction With Local Deformations

This last minimization procedure is made with θ previously estimated and now fixed to find the optimal local deformation parameters of the complete model.

The energy function to be minimized is just a final refinement of the global deformations applied to the mean shape, since the main deformation modes have been captured by the PCA-based global prior knowledge of each vertebra. For this section, we use the following deterministic procedure.

- For each point p_i of the vertebra shape model s ($s = (p_1, p_2, \ldots p_i, \ldots, p_n)^T$ with $p_i = (x_i y_i z_i)^T$), and until $E(\hat{s}(\theta))$ is stable.
- The model energy $E(\hat{s}(\theta))$, expressed by (9) is evaluated for different positions of p_i (namely; $p_i + \delta p_i$, p_i, and $p_i - \delta p_i$) along its normal. The normal is estimated by computing the average of the normal of all facets to which the vertex belongs.
- We retain the configuration associated with the lowest energy.

In order to speed up this local deterministic optimization procedure, we start with a given and over estimated value for δp_i until $E(\hat{s}, \theta)$ become stable and we run the procedure successively with decreasing values of δp_i (e.g., Fig. 6).

In order to speed up this local deterministic optimization procedure, we start with a given, an overestimated value for δp_i until $E(\hat{s}, \theta)$ becomes stable and we run the procedure successively with decreasing values of δp_i (e.g., Fig. 6).

VI. Validation of 3-D Reconstruction

Validation of 3-D reconstruction accuracy is a difficult task because a scanned spine database is generally not available.

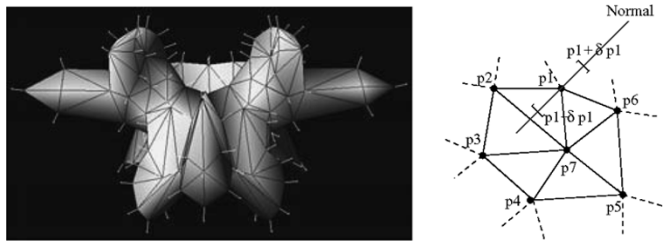

Fig. 6. Local deformations. (a) normal at the control points, (b) movement of point p1 along its normal.

Visual examination is the most obvious method for evaluation of the 3-D reconstruction accuracy, but can be considered as an informal and insufficient approach. We have 13 spine segments[4] containing altogether 57 (6 lumbar and 51 thoracic) vertebrae. These 13 vertebrae segments were scanned with a CT-scan device. Each CT slice of 1 mm thickness was taken with a resolution of 512 × 512 pixels and 12 bits per pixel. The CT scan reconstruction was made by piling the CT slices of the vertebrae[5] [44] using SliceOmatic software. This software allows one to automatically segment the CT-scan slices and then to correct the automatic segmentation manually to distinguish the different objects in the initial image. The accuracy of this technique is evaluated at ±1 mm [45] and it allows a CT scan reconstruction of the vertebrae containing up to 7000 points. Twelve landmarks (extremities of pedicles, extremities of the diameter of the spinal canal) were identified on each vertebra using an interactive graphical computer tool. These landmarks were then used to calculate the dimensions of the pedicles and the spinal canal[6] (width and depth). The validation technique consists of fitting the model of our 3-D reconstruction method to the corresponding scanned vertebra. This 3-D reconstruction method is used to estimate the mean and the maximum error distance between the 3-D reconstructed model and the corresponding scanned model. The results of the comparisons will be expressed as *point to surface*, i.e., each point of reconstructed vertebra is projected onto the surface on the corresponding scanned vertebra and the point-surface euclidean distance is computed.

[4]Thirteen scoliotic patients of Sainte-Justine Hospital in Montreal, Canada, participated in this study. Most of the patients were adolescents, ranging from 11 to 21 years old; all were female. They all had idiopathic thoracic or thoraco-lumbar scoliosis, with Cobb angles ranging from 3° to 52°. As the surgical planning for these patients had required computed tomography (CT) scans of some strategic vertebrae to obtain 3-D reconstructions, we analyzed only these vertebrae.

[5]The CT scan reconstruction was made by piling the segmented CT slices of the vertebrae using the marching cube algorithm. the marching cube algorithm is used in volume rendering to reconstruct an isosurface from a 3-D field of values. The basic principle is to subdivide space into a series of small cubes. The algorithm then instructs us to "march" through each of the cubes testing the corner points and replacing the cube with an appropriate set of triangles. The result is a smooth surface that approximates the isosurface. The user can change the selected threshold value, making use of a simple graphical interface. The accuracy was defined by estimating the errors on shape between the scanned segmented vertebra and the corresponding model obtained by direct measurement using Fastrack.

[6]The estimation of these morphometric parameters are useful for the pedicle insertion during a typical surgical intervention of scoliosis.

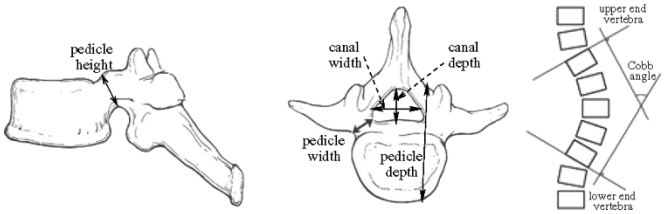

Fig. 7. Morphometric parameters used in our validation protocol.

We also considered the Cobb[7] angle, related to the curve of the spinal column (e.g., Fig. 7).

VII. Experimental Results

A. Vertebra Database

The vertebra database, used in our application, includes 1020 thoracic and lumbar vertebrae (30 normal and 30 scoliotic for each vertebral level, i.e., 5 lumbar and 12 thoracic). These data were obtained by digitization of the anatomical points on anatomical specimens selected in the Hamann Todd osteology collection, Cleveland, OH, and Smithsonian Institution in Washington, DC [46][8] Fastrack (POLHEMUS, A Rockwell Collins Company) is the name of the electromagnetic device used to digitize each vertebra by means of a pointer. The accuracy of this device is evaluated at ± 0.2 mm [47]. The 3-D coordinates of the pointer were recorded in a specific reference system. Let us recall that the digitizing protocol consisted of measuring specific anatomical landmarks on each vertebra, thus creating a set of approximately 200 points depending on the level measured with regard to its particular geometry [34]. Different points were acquired in a specific order and recorded in this sequence. After the measurements were done, each vertebra was then reconstructed using computer graphics software developed by our Imaging and Orthpopedics Research laboratory in Montreal, Canada. This computer graphics software is based on a protocol making it possible to take into account the topology of a vertebra which describe how the triangles are connected and the geometry of the vertebra which is the specification of the precise location of the vertices. Each set of points was then re-localized in a local coordinate system.[9]

B. Comparison Protocol

In our application, we use the comparison protocol described in [25]. Three-dimensional reconstruction models of the vertebrae contain up to 7000 points per vertebra and will constitute the ground truth for our validation procedure. First, the validation procedure consists of fitting the model of 200 points of our 3-D reconstruction method on the scanned and segmented vertebra. To this end, we use 12 landmarks (extremities of pedicles, extremities of the diameter of the spinal canal) on the reconstructed model whose position is known, and we estimate the rigid transformation allowing us to pass from the set of anatomical landmarks of our reconstructed model to the set of corresponding anatomical landmarks previously extracted from the scanned model. Then, we apply this rigid transformation to all points of the reconstructed vertebra. Once this is done, we optimize the rigid transformation, which enables us to readjust the two models of vertebra. Optimization consists of finding neighbors on the scanned vertebra to each point of the reconstructed vertebra and then of estimating and re-applying the rigid deformation, allowing us to pass from the set of points of the reconstructed vertebra to the set of points close to the scanned vertebra. This procedure is repeated until the difference in variation of error between two successive stages is lower than a given threshold.

This comparison was made using the distance (mean, root mean square (RMS), and maximum) between a point from the reconsructed vertebra and the surface of the corresponding vertebra obtained with CT-scan, whose accuracy is ± 1 mm [45].

C. Experimental Results

We have validated our 3-D reconstruction method on 13 scoliotic thoracic spine segments CT and 13 pairs of calibrated radiographic images (postero-anterior and lateral) associated to this spine segment (a subset of our database of 30 scoliotic pairs). We use an efficient way of calculating the eigenvectors associated with non zero eigenvalues as given in [24]. The first m ($m \in \{8, 9, 10\}$, depending of the vertebra level) eigenmodes $\{(\lambda_1, \phi_1), \ldots, (\lambda_m, \phi_m)\}$ are chosen to cover at least 90% of the population's variability. For the experiments, we have chosen $\beta = 0.02$ for the weighting factor penalizing the prior energy term with respect to external energy for Section V-C and Section V-D, $\mu = 90$ and $\nu = 8$ for the variance parameters of the local deformation model. These different threshold values have been chosen empirically after a set of experiments from a database of 30 pairs of calibrated radiographic images of scoliotic spine (by trials and errors after visual examinations of the postero-anterior and lateral segmented contours) and with an optimization procedure ensuring the global minimum (i.e., with E/S algorithm). The 13 pairs of calibrated radiographic images of scoliotic spine associated to 13 scoliotic spine segments CT used for these validation experiments are a subset of this database of 30 pairs. These different parameters (β, μ and ν) are valid for this imaging modality. We used the Canny edge detector to estimate the edge map which is then used for estimation of the edge *potential field* on the two radiographic views (used in the likelihood energy term). In our application, $\sigma = 1$, mask size is 5×5, and the lower and upper thresholds are given by the semi-automatic estimation technique[10] proposed in [37].

We have implemented the E/S and GAs in C++ and compared the execution times of these algorithms (e.g., Figs. 8 and 9). In our application, parameters of GA are the

[7]Cobb angle is used to quantify the scoliosis deformation by evaluating the spinal curve relatively to the postero-anterior radiographic view.

[8]Age, sex, race, height, weight, cause of death and peculiar dissection findings of each scoliotic specimen are available.

[9]To our knowledge, the vertebrae base is the largest database available in the literature [46].

[10]This technique allows to estimate the lower τ_l and upper τ_h thresholds of the hysteresis thresholding step of the canny procedure in the following way; We set $\tau_l = 0.5\,\tau_h$ and τ_h is estimated as being the value of the gradient module for which the repartition function of the gradient module (computed on the whole image) reaches a certain threshold value p_h ($p_h < 1$). This procedure allows to make the canny procedure dependent on only one threshold, p_h which is closely related to the percentage of edge that will be detected in the image. In our application, we use $p_h = 0.8$ and this technique and the choice of p_h turned out to be reliable in our application.

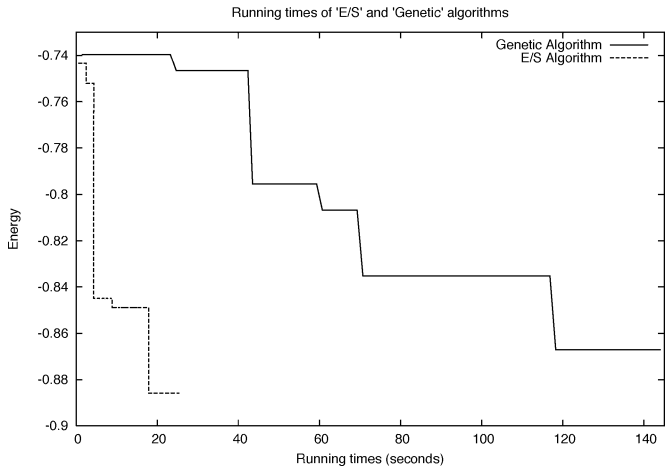

Fig. 8. Running times of E/S and GAs as a function of the energy.

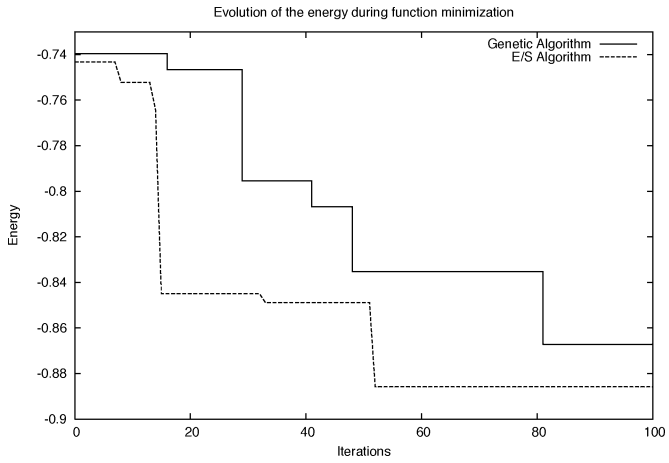

Fig. 9. Evolution of the energy during function minimization for E/S and GAs.

following; population size $=$ 100, crossover rate $=$ 0.80, mutation rate $=$ 0.01, maximum number of generations $=$ 100. Each of $7+m$ parameters θ_i is quantified on 8 bits. Parameters of E/S algorithm are the following; population size $=$ 100, diameter of the exploration graph $=$ 32, maximum number of generations $=$ 100. Figs. 8 and 9 display the running times of E/S and GAs as a function of the energy and the evolution of the energy during the optimization process for E/S and GAs as a function of the number of iterations, respectively, for a given vertebral level. These figures shows the E/S and GAs take about 55 and 80 generations (or 28 and 120 s), respectively, to converge to a good estimate for a given vertebral level (with Linux running on a 2.0 GHz AMD Atlon PC workstation with 1 GByte of memory). In fact, the convergence rate can vary significantly depending on the complexity of the energy function $E(s,\theta)$ to be minimized (or the quality of the input radiographic images). Nevertheless, in all tested cases, we obtain better minima and convergence with the E/S comparatively to the GA (see Table I). Fig. 10 shows the projection of the cube template on corresponding vertebral body on postero-anterior and lateral views obtained for the extreme values of position t, scale vector k and orientation α of the restricted search space initially defined for the cube

TABLE I
EXAMPLE OF MINIMA OBTAINED WITH E/S AND GAS ALGORITHMS FOR LUMBAR AND THORACIC VERTEBRAE

Optimization	Vertebral level	
	Lumbar	Thoracic
E/S	$E=-0.89$	$E=-0.87$
Genetic	$E=-0.87$	$E=-0.82$

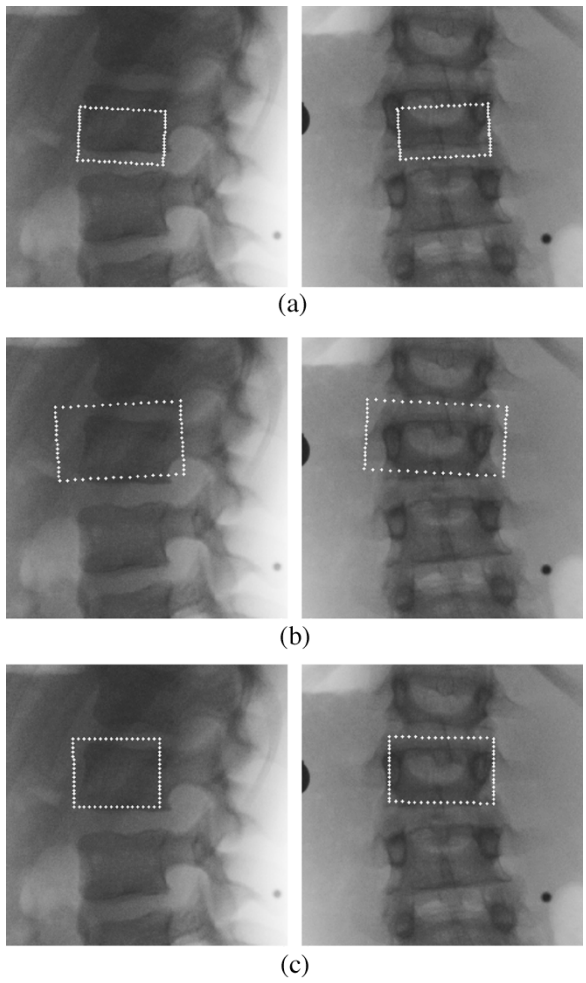

Fig. 10. Projection of the cube template on corresponding vertebral body on postero-anterior and lateral views obtained for the extreme values of position t, scale vector k and orientation α. (a) $k=(0.8,0.8,0.8)$, $\alpha=(-3,-3,-3)$, and $t=(-2,-2,-2)$; (b) $k=(1.3,1.3,1.3)$, $\alpha=(3,3,3)$, and $t=(2,2,2)$; and (c) final reconstruction of the cube, $k=(0.90,0.98,1.22)$, $\alpha=(0.80,0.17,-1.42)$, and $t=(1.72,0.13,2.28)$.

template (see Section II-A) and its final reconstruction after E/S optimization.

Fig. 11 shows the projection of the vertebra template on corresponding vertebra on postero-anterior and lateral views obtained for the extreme values of position t, scale vector k and orientation α and the final reconstructed vertebra after GA and E/S optimization.

Fig. 12 shows the estimated reconstructed L2 vertebra when local deformations are taken into account to refine the reconstruction obtained in Fig. 11. The local deformation process can efficiently adjust the deformable template to the presegmented

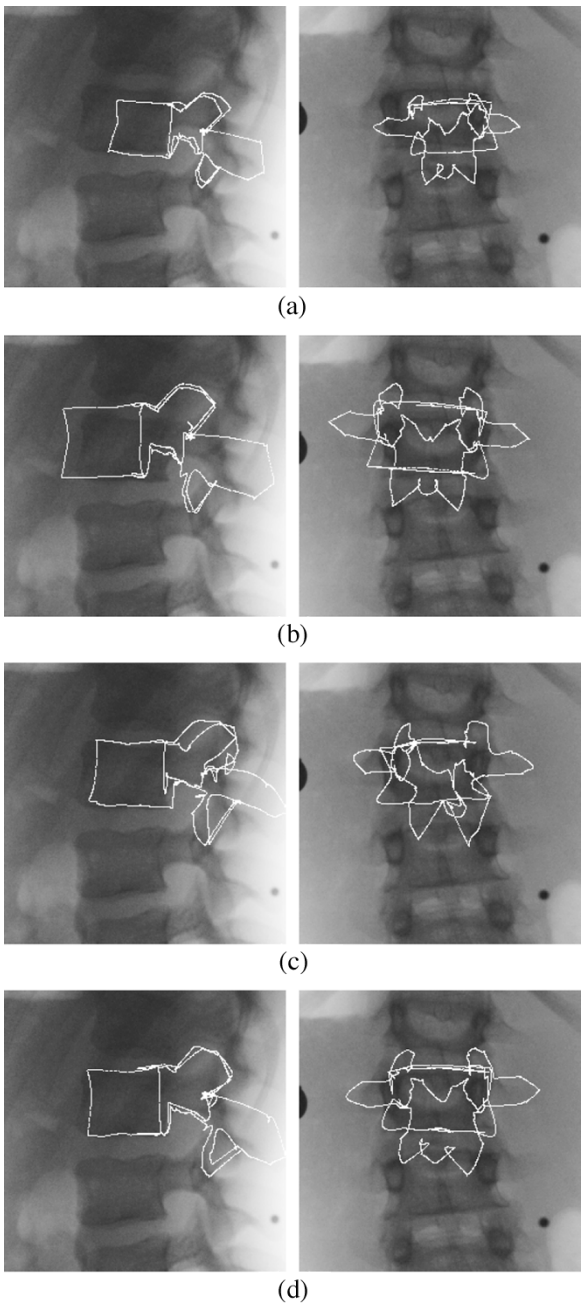

Fig. 11. Projection of the L2 vertebra template on corresponding vertebra postero-anterior and lateral views when position t, scale k and orientation α take the least and the greatest values in a corresponding search interval: (a) $k = 0.86$, $\alpha = (-4, -4, -4)$, and $t = (-3, -3, -3)$; (b) $k = 1.30$, $\alpha = (4, 4, 4)$, and $t = (3, 3, 3)$; (c) final reconstruction of the vertebra, $k = 0.96$, $\alpha = (0.5, -2.5, 0.5)$, $t = (1.1, -1.5, 1.0)$, and $b = (-5, 10, 15, -5, -5, 0, 0, 0, 5)$ with GA optimization; and (d) final reconstruction of the vertebra, $k = 0.97$, $\alpha = (0.50, -1.05, 0.49)$, $t = (1.03, -1.49, 1.00)$, and $b = (-5.35, 8.45, 14.69, -7.06, -5.05, 11.08, 5.43, -0.87, 4.10, -6.64)$ with E/S optimization.

contours of each radiographic image leading to a better 3-D reconstruction result.

Table II presents (mean, root mean square (RMS), and maximum) errors between points from the reconstructed vertebra and the surface of the corresponding scanned vertebra for different vertebral levels. These errors are, respectively, (1.46 $\pm$ 1.47) mm, (1.87 $\pm$ 0.23) mm, and (5.35 $\pm$ 0.93) mm for lumbar vertebrae, and (1.30 $\pm$ 1.32) mm, (1.66 $\pm$ 0.25) mm, and (4.64 $\pm$ 0.84) mm for thoracic vertebrae. We also calculated these errors without local deformations. These errors are then (1.58 $\pm$ 1.32) mm, (1.92 $\pm$ 0.31) mm, and (5.82 $\pm$ 0.63) mm for lumbar vertebrae, and (1.46 $\pm$ 1.23) mm, (1.71 $\pm$ 0.35) mm, and (5.07 $\pm$ 0.71) mm for thoracic vertebrae.

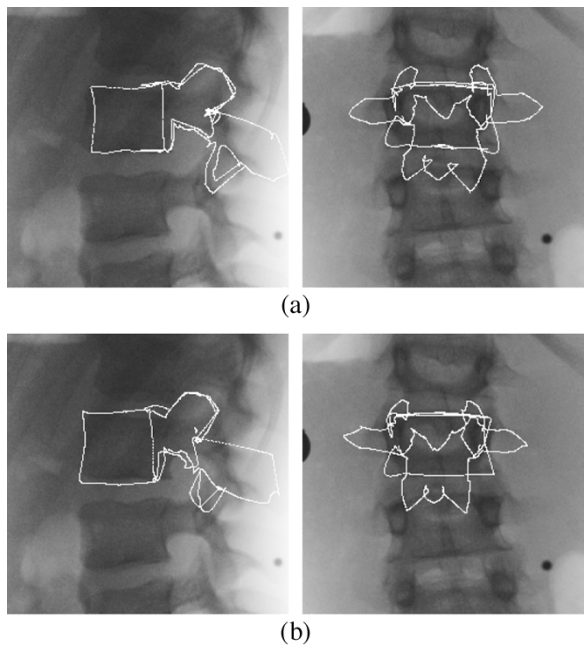

Fig. 12. Global and local deformations on L2 vertebra template. (a) Globally deformed shape $E = -0.79$. (b) Globally and locally deformed shape $E = -0.88$.

Table III presents width, height, and depth of spinal pedicles and canal differences between the reconstructed model resulting from our 3-D reconstruction method and the model resulting from CT-scan. The elements of the table denote the mean of N absolute values of the difference between the measure of morphometric parameter on reconstructed vertebra and the corresponding measure on scanned vertebra. Table IV presents the Cobb angle of projections of vertebral end-plates of these reconstructed vertebra segments with the corresponding end-plates of these reconstructed vertebrae manually calculated by an expert from Sainte-Justine Hospital (Montréal, Canada) on a postero-anterior X-ray image.

Figs. 13–15 show a few examples of 3-D reconstruction of vertebra segments of some scoliotic spines.

To compare these results with those presented in [31], we note that the precision of the 3-D/2-D registration method presented in [31] remains better than the precision of the 3-D reconstruction method described in this paper (see Table VIII). This is due to the fact that the method presented in [31] is widely supervised and requires the knowledge of the position of six anatomical points (namely, the center of the superior and inferior end-plates, the upper and lower extremities of both pedicles) to initialize the 3-D reconstruction process of each vertebra of the spine i.e., the knowledge of the position of 102 anatomical points for the 3-D reconstruction of the vertebra segment (L5/. . ./T1) while the proposed 3-D reconstruction method only

TABLE II
RESULTS ON POINT-TO-SURFACE COMPARISONS OF 57 SCOLIOTIC VERTEBRAE. N DENOTES THE TOTAL NUMBER OF VERTEBRAE AT DIFFERENT VERTEBRAL LEVELS. ALL DATA ARE SHOWN AS MEAN ± STANDARD DEVIATION

Vertebral level	N	Mean error (mm)	Root mean square (mm)	Maximum error (mm)
Thoracic				
T6	3	1.17±1.22	1.48±0.13	4.27±0.55
T7	6	1.32±1.38	1.68±0.33	5.00±1.06
T8	9	1.28±1.28	1.64±0.23	4.66±0.60
T9	10	1.33±1.34	1.70±0.23	4.79±0.75
T10	9	1.23±1.28	1.59±0.14	4.41±0.80
T11	9	1.30±1.31	1.63±0.31	4.43±0.95
T12	5	1.30±1.25	1.66±0.41	4.20±1.04
Lumbar				
L1	2	1.33±1.27	1.67±0.33	4.57±0.84
L2	1	1.70±1.60	2.15±0.00	5.70±0.00
L3	2	1.30±1.30	1.75±0.35	5.20±1.70
L5	1	1.50±1.70	1.93±0.25	5.95±1.20

TABLE III
RESULTS ON COMPARISONS OF 57 SCOLIOTIC VERTEBRAE. N DENOTES THE TOTAL NUMBER OF VERTEBRAE AT DIFFERENT VERTEBRAL LEVELS. ALL DATA ARE SHOWN AS MEAN ± STANDARD DEVIATION

Vertebral level	N	Pedicle			Canal	
		width (mm)	height (mm)	depth (mm)	depth (mm)	width (mm)
Thoracic						
T6	3	1.90±0.96	2.37±0.74	0.36±0.26	1.55±0.65	1.15±0.79
T7	6	1.74±1.09	1.41±1.00	0.76±0.71	2.87±1.17	0.56±0.78
T8	9	1.58±0.88	1.45±1.03	0.65±0.46	1.45±0.78	1.55±1.23
T9	10	1.55±0.83	1.44±0.91	0.69±0.76	1.62±1.11	1.66±1.28
T10	9	1.32±0.91	0.63±0.66	0.49±0.50	1.07±0.76	1.96±1.25
T11	9	1.39±0.51	1.03±0.93	0.57±0.43	1.22±0.97	1.52±1.14
T12	5	2.05±1.69	0.61±0.36	1.07±1.11	1.51±0.88	1.98±1.35
Lumbar						
L1	2	1.88±1.02	1.50±1.32	1.11±0.58	1.06±0.88	2.43±1.45
L2	1	0.76±0.00	1.33±0.00	1.34±0.00	1.91±0.00	1.55±0.00
L3	2	2.09±0.63	0.78±0.88	1.48±0.70	0.57±0.15	1.78±1.02
L5	1	2.34±0.17	1.78±0.79	0.32±0.30	0.98±0.78	1.79±0.21

TABLE IV
COBB ANGLE OF PROJECTIONS OF VERTEBRAL END-PLATES OF THESE RECONSTRUCTED VERTEBRA SEGMENT WITH THE CORRESPONDING END-PLATES OF THESE RECONSTRUCTED VERTEBRAE MANUALLY CALCULATED BY AN EXPERT FROM SAINTE-JUSTINE HOSPITAL (MONTRÉAL, CANADA) ON A POSTERO-ANTERIOR X-RAY IMAGE

Vertebra segment	No Patient	Cobb angle	
		Projections of vertebra segment (deg)	Postero-anterior X-ray image (deg)
T10 - T12	1	3	3
T10 - T12	2	11	13
T11 - T12	3	15	14
T6 - T11	4	45	43
T6 - T11	5	40	42
T7 - T12	6	46	43
T7 - T10	7	39	42
T7 - T11	8	50	52
T8 - T11	9	38	36
T6 - T9	10	33	32
T7 - T9	11	40	42
T7 - T9	12	34	32
T8 - T9	13	31	29

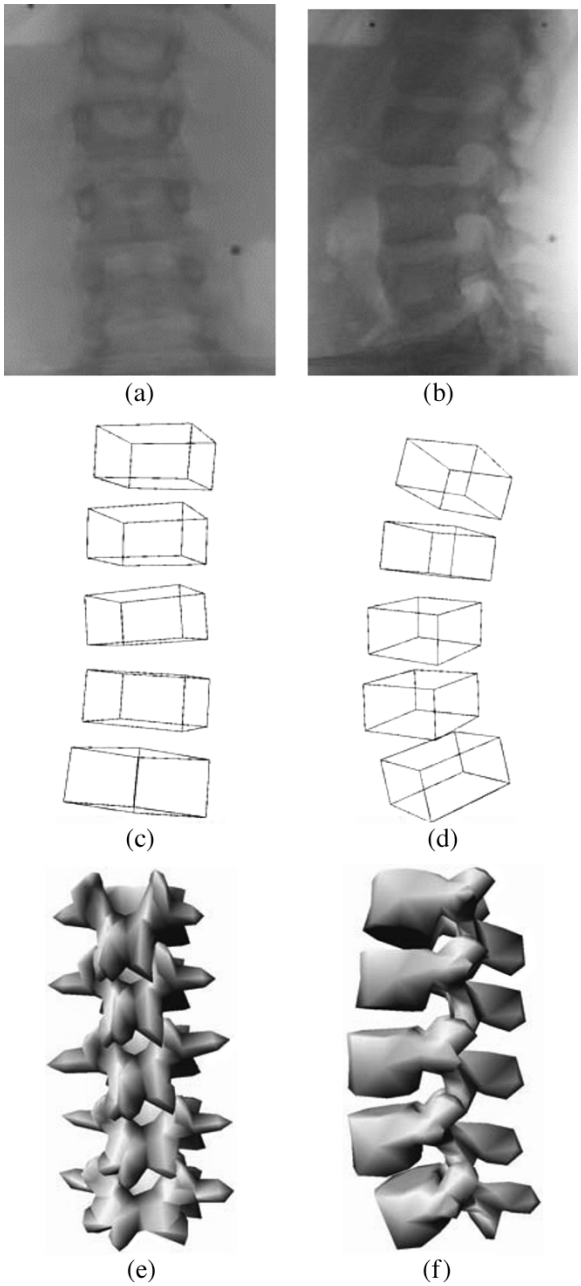

Fig. 13. Three-dimensional reconstruction of vertebra segment (L1/L2/L3/L4/L5) of a given scoliotic spine. (a) Postero-anterior image, (b) lateral image, (c) and (d) visualization of the reconstructed cube segment (L1/L2/L3/L4/L5) from the coronal and sagittal views. (e) and (f) Visualization of reconstructed vertebra segment (L1/L2/L3/L4/L5) from the coronal and sagittal views.

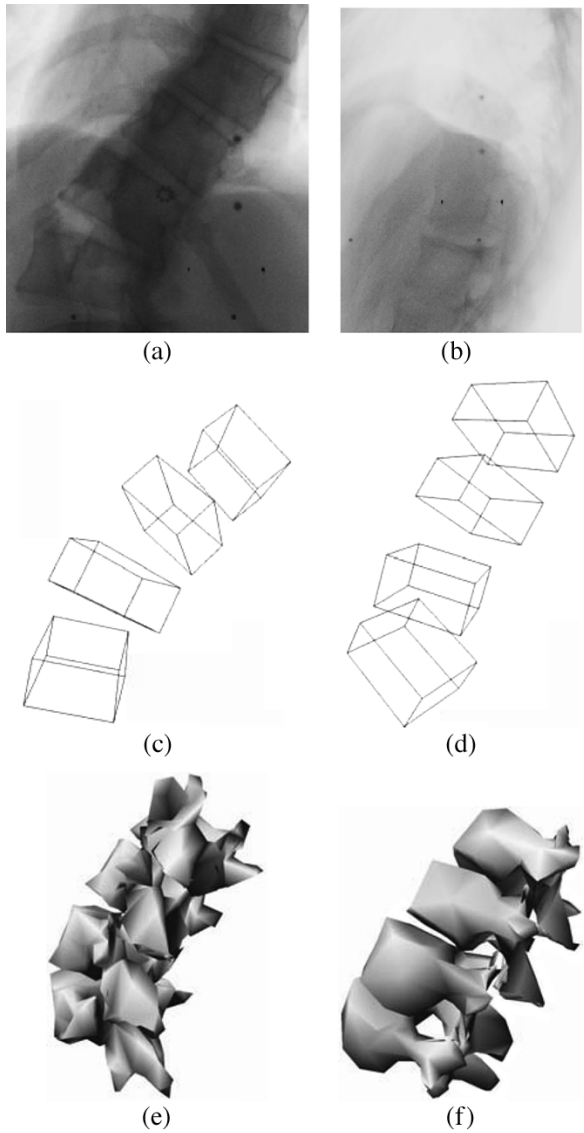

Fig. 14. Three-dimensional reconstruction of vertebra segment (T10/T11/T12/L1) of a given scoliotic spine. (a) Postero-anterior, (b) lateral image, (c) and (d) visualization of the reconstructed cube segment (T10/T11/T12/L1) from the coronal and sagittal views. (e) and (f) Visualization of reconstructed vertebra segment (T10/T11/T12/L1) from the coronal and sagittal views.

requires two points, namely the superior and inferior end-plates, of the vertebra segment to be defined. The validation results presented above show that the accuracy of our 3-D hierarchical reconstruction method is comparable to CT-scan 3-D reconstruction.

Tables V and VI show the results of computing the mean and maximum error distances $\overline{x}$, standard deviation σ, and confidence interval for samples of size n from the vertebra database. We assume that the vertebra database is approximately normal. A $100(1-\alpha)\%$ confidence interval is $[\overline{x} - t_{\alpha/2}(\sigma/\sqrt{n}), \overline{x} + t_{\alpha/2}(\sigma/\sqrt{n})]$ where $t_{\alpha/2}$ is the upper $\alpha/2$ point of the t distribution with degrees of freedom $n-1$. Selecting $\alpha = 0.05$, we find the value of $t_{0.025}$ with 5 degrees of freedom is 2.571 for lumbar vertebrae and 50 degrees of freedom is 2.00 for thoracic vertebrae, so the 95% confidence interval is $\overline{x} \pm 2.571(\sigma/\sqrt{5})$ for lumbar vertebrae and $\overline{x} \pm 2.00(\sigma/\sqrt{50})$ for thoracic vertebrae.

To test the right hypotheses of the statistical significance of these local deformations relatively to the global deformations (with a level of significance $\alpha = 0.05$), the Student's t-test, namely, $T = (\sqrt{n}/\sigma)\overline{x}$ has to be lower then $t_{\alpha/2}$ (i.e., $|T| \leq t_{\alpha/2}$) [48]. Table VII, thus, shows that local deformations give a significant improvement in the accuracy of reconstruction except in the case of lumbar vertebrae (probably due to the low size of the validation set for the lumbar vertebrae).

The experiments have shown that the results obtained with local deformations are better than the results obtained without

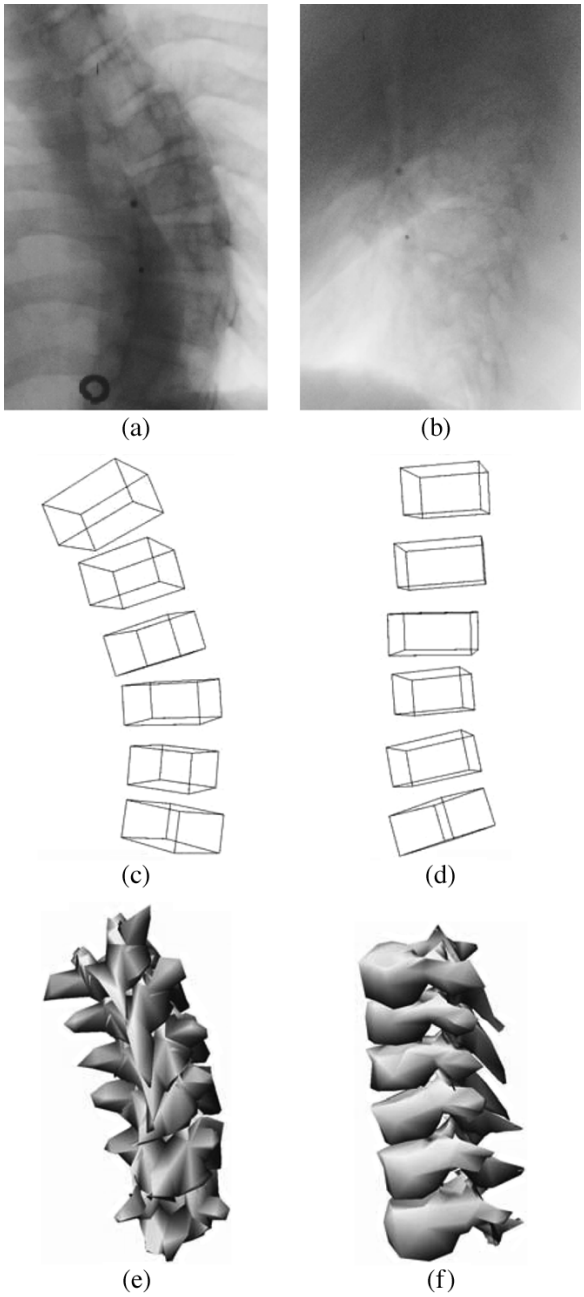

Fig. 15. Three-dimensional reconstruction of vertebra segment (T6/T7/T8/T9/T10/T11) of a given scoliotic spine. (a) Postero-anterior image, (b) lateral image, (c) and (d) visualization of the reconstructed cube segment (T6/T7/T8/T9/T10/T11) from the coronal and sagittal views. (e) and (f) Visualization of reconstructed vertebra segment (T6/T7/T8/T9/T10/T11) from the coronal and sagittal views.

local deformations (see Table V and VI). This is due to the fact that our PCA does not model 100% of the scoliotic deformations of our vertebra database and that our vertebra database is not big or representative enough (i.e., 30 normal and 30 scoliotic vertebra shapes does certainly not contain all the possible scoliotic deformations for each vertebral level).

Let us note that the estimated global deformation parameters after 3-D reconstruction (i.e., parameter vector b, setting the amplitude of each deformation mode of the scoliotic deformation) and the measures of morphometric parameters can also be used to quantify the scoliosis, its nature or to analyze the improvement of orthopedic or surgical corrections. Let us also note that the resulting 3-D reconstructed spine can also be efficiently exploited as prior knowledge and geometric constraints for the problem of the rib cage reconstruction. This will be the topic of our futur research.

VIII. Discussion and Conclusion

We have presented an original coarse-to-fine approach for the 3-D reconstruction of the scoliotic spine using contours extracted from biplanar radiographic images and *a priori* hierarchical global knowledge both of the geometrical structure of the whole spine and of the statistical structure of each vertebra. From an algorithmic point of view, the reconstruction problem is decomposed in two optimization problems of reduced complexity allowing us to drastically save computational effort and/or provide accelerated convergence toward an improved estimate. In our application, these two optimization problems are efficiently solved with a stochastic optimization procedure (i.e., with E/S algorithm). This optimization procedure is fast compared to other minimization techniques such as the gradient-based method and GA. This method has been tested on a sample of 30 pairs of radiographic images demonstrating its efficiency and robustness.

Let us recall that this 3-D reconstruction method is used to estimate the mean and the maximum error distance between the 3-D reconstructed model and the corresponding scanned model. The results of the comparisons will be expressed as *point to surface*, i.e., each point of reconstructed vertebra is projected onto the surface on the corresponding scanned vertebra and the point-surface euclidean distance is computed. We also considered the Cobb angle, related to the curve of the spinal column.

The mean error is (1.46 ± 1.47)mm for lumbar vertebra and (1.30 ± 1.32)mm for thoracic vertebra. The maximum error is (5.35 ± 0.93)mm for lumbar vertebra and (4.64 ± 0.84)mm for thoracic vertebra for our 3-D reconstruction technique.

Let us also note that there are many other morphometric parameters to evaluate the quality of the reconstructed scoliotic spine by using Cobb angle in the frontal view of each curvature, vertebral axial rotation on frontal plane deformity, angle of plane of maximum curvature, apical vertebra frontal plane, etc.

The most computationally intense step in our coarse-to-fine optimization strategy is the fine reconstruction involving local deformations. In this step, we evaluate the model energy for different candidate positions (three positions) and for each point (200 points) of the vertebra shape. This procedure is repeated several times.

A validation in computer simulations and/or projections from the CT data could have been performed but we have chosen not to do so.

The proposed scheme, thus, constitutes an alternative to CT-scan 3-D reconstruction with the advantage of low irradiation and will be of great interest for evaluation of spinal deformities, simulation of orthopaedic treatments, and for reliable geometric models for finite element studies. However,

TABLE V
THE MEAN ERROR DISTANCES, STANDARD DEVIATION, AND CONFIDENCE INTERVAL OBTAINED FROM THE PROPOSED METHOD WITH AND WITHOUT LOCAL DEFORMATIONS FOR THE LUMBAR AND THORACIC VERTEBRAE

		Proposed method	
		without local deformation	with local deformation
Mean (mm)	Lumbar	1.58	1.46
	Thoracic	1.46	1.30
Standard deviation (mm)	Lumbar	1.32	1.47
	Thoracic	1.23	1.32
Confidence interval (mm)	Lumbar	[0.19 , 2.97]	[0.00 , 3.00]
	Thoracic	[1.12 , 1.80]	[0.93 , 1.67]

TABLE VI
THE MAXIMUM ERROR DISTANCES, STANDARD DEVIATION, AND CONFIDENCE INTERVAL OBTAINED FROM THE PROPOSED METHOD WITH AND WITHOUT LOCAL DEFORMATIONS FOR THE LUMBAR AND THORACIC VERTEBRAE

		Proposed method	
		without local deformation	with local deformation
Maximum error (mm)	Lumbar	5.82	5.35
	Thoracic	5.07	4.64
Standard deviation (mm)	Lumbar	0.63	0.93
	Thoracic	0.71	0.84
Confidence interval (mm)	Lumbar	[5.16 , 6.48]	[4.37 , 6.33]
	Thoracic	[4.87 , 5.27]	[4.40 , 4.88]

TABLE VII
RESULTS OF STUDENT'S t-TEST ABOUT STATISTICAL SIGNIFICANCE OF THE LOCAL DEFORMATIONS

T-Test of the		size	degrees of freedom	$\mid T \mid$	$t_{0.025}$	Student's t-test
Mean	Lumbar	6	5	2.43	2.57	No
	Thoracic	51	50	7.03	2.00	Yes
Maximum error	Lumbar	6	5	14.09	2.57	Yes
	Thoracic	51	50	39.45	2.00	Yes

TABLE VIII
THE MEAN AND MAXIMUM ERROR DISTANCES OBTAINED FROM THE SUPERVISED METHOD DESCRIBED IN [31] AND THE PROPOSED METHOD (DESCRIBED IN THIS PAPER) FOR THE LUMBAR AND THORACIC VERTEBRAE. ALL DATA ARE SHOWN AS MEAN $\pm$ STANDARD DEVIATION

	Mean error (mm)		Maximum error (mm)	
	Lumbar	Thoracic	Lumbar	Thoracic
Supervised method [31]	0.71 ± 0.06	1.48 ± 0.27	3.67 ± 0.80	6.44 ± 1.76
Proposed method	1.46 ± 1.47	1.30 ± 1.32	5.35 ± 0.93	4.64 ± 0.84

this reconstruction method is not suitable without improvement for surgical navigation applications when compared to CT-scan reconstruction errors of ± 1 mm, the gold standard for those applications.

The proposed method remains sufficiently general to be applied to other medical reconstruction problems (i.e., rib cage, pelvis, knee, etc.) for which the database of this anatomical structure is available (with two or more radiographic views).

ACKNOWLEDGMENT

The authors would like to thank the anonymous reviewers for helpful comments and criticisms which have greatly improved the paper.

REFERENCES

[1] V. N. Cassar-Pullicino and S. M. Eisenstein, "Imaging in scoliosis: what, why and how?," *Clin. Radiol.*, vol. 57, no. 7, pp. 543–562, July 2002.
[2] W. Lorensen and H. Cline, "Marching cubes: a high resolution 3-D surface construction algorithm," *Comput. Graphics*, vol. 21, no. 4, pp. 163–169, 1988.
[3] C. Lorenz and N. Krahnstöver, "Generation of point-based 3-D statistical shape models for anatomical objects," *Comput. Vis. Image Understanding*, vol. 77, pp. 175–191, 2000.
[4] J. Lötjönen, P.-J. Reissman, I. Magnin, and T. Katila, "Model extraction from magnetic resonance volume date using the deformable pyramid," *Med. Image Anal.*, vol. 3, no. 4, pp. 387–406, 1999.
[5] S. Sandor and R. Leadhy, "Surface-based labeling of cortical anatomy using a deformable atlas," *IEEE Trans. Med. Imag.*, vol. 16, no. 1, pp. 41–54, Feb. 1997.
[6] J. Novosad, F. Cheriet, Y. Petit, and H. Labelle, "Three-dimensional 3-D reconstruction of the spine from a single X-ray image and prior vertebra models," *IEEE Trans. Biomed. Eng.*, vol. 51, no. 9, pp. 1628–1639, Sep. 2004.

[7] R. Medina, M. Garreau, J. Toro, J. Coatrieux, and D. Jugo, "Three-dimensional reconstruction of the left ventricle from two angiographic views: an evidence combination approach," *IEEE Trans. Syst., Man Cybern., Pt. A*, vol. 34, no. 3, pp. 359–370, May 2004.

[8] A. L. Bras, S. Laporte, D. Mitton, J. de Guise, and W. Skalli, "Three-dimensional (3D) detailed reconstruction of human vertebrae from low-dose digital stereoradiography," *Eur. J. Orthop. Surg. Traumatol.*, vol. 13, no. 2, pp. 57–62, June 2003.

[9] W. Martin and J. Aggarwal, "Volumetric descriptions of objects from multiple views," *IEEE Trans. Pattern Anal. Mach. Intell.*, vol. PAMI-5, no. 2, pp. 150–158, Feb. 1983.

[10] L. Caponetti and A. Fanelli, "Computer-aided simulation for bone surgery," *IEEE Comput. Graphics Applicat.*, vol. 13, no. 6, pp. 86–92, 1993.

[11] R. Benjamin, "Object-based 3-D X-ray imaging," in *Proc. Computer Vision, Virtual Reality and Robotics in Medicine*, Paris, France, 1995, pp. 444–448.

[12] D. Terzopoulos, A. Witkin, and M. Kass, "Constraints on deformable models: recovering 3-D shape and nonrigid motion," *Artif. Intell.*, vol. 36, no. 1, pp. 91–123, 1988.

[13] E. Bardinet, L. Cohen, and N. Ayache, "A parametric deformable model to fit unstructured 3-D data," *Comput. Vis. Image Understanding*, vol. 71, no. 1, pp. 39–54, 1998.

[14] B. Nikkhade-Dehkordi, M. Bro-Nielsen, T. Darvann, C. Gramkow, N. Egund, and K. Hermann, "3-D reconstruction of the femoral bone using two X-ray images from orthogonal views," in *Comput. Assist. Radiol.*, Jun. 26–29, 1996, p. 1015.

[15] Y. Kita, "Elastic-model driven analysis of several views of a deformable cylindrical object," *IEEE Trans. Pattern Anal. Mach. Intell.*, vol. 18, no. 12, pp. 1150–1162, Dec. 1996.

[16] G. T. Marzan, "Rational design for close-range photogrammetry," Ph.D. dissertation, Dept. Civil Eng., Univ. Illinois at Urbana-Champaign, 1976.

[17] J. Dansereau and I. Stokes, "Measurements of the three-dimensional shape of the rib cage," *J. Biomech. Eng.*, vol. 21, pp. 893–901, 1988.

[18] S. Delorme, Y. Petit, J. de Guise, H. Labelle, C. Aubin, and J. Dansereau, "Assessment of the 3-D reconstruction and high-resolution geometrical modeling of the human skeletal trunk from 2-D radiographic images," *IEEE Trans. Biomed. Eng.*, vol. 50, no. 8, pp. 989–999, Aug. 2003.

[19] D. Mitton, C. Landry, S. Veron, W. Skalli, F. Lavaste, and J. A. D. Guise, "3-D reconstruction method from biplanar radiography using nonstereocorresponding points and elastic deformable meshes," *Med. Biol. Eng. Comput.*, vol. 38, pp. 133–139, 2000.

[20] E. Marcil, J. Dansereau, H. Labelle, and J. D. Guise, "Incorporation of patient displacement into a trunk reconstruction technique," in *Proc. Int. Conf. IEEE Engineering in Medicine and Biology Society*, vol. 1, Sep. 1995, pp. 385–386.

[21] S. Lavallée, L. Brunie, B. Mazier, and P. Cinquin, "Matching of medical images for computed and robot assisted surgery," in *Proc. Int. Conf. IEEE Engineering in Medicine and Biology Society*, vol. 1, 1991, pp. 39–40.

[22] P. Besl and H. McKay, "A method for registration of 3-D shapes," *IEEE Trans. Pattern Anal. Mach. Intell.*, vol. 14, no. 2, pp. 239–256, Feb. 1992.

[23] M. Fleute and S. Lavallée, "Nonrigid 3-D/2-D registration of images using a statistical model," in *Medical Image Computing and Computer-Assisted Intervention*. Berlin, Germany: Springer-Verlag, 1999, vol. 38, pp. 138–147.

[24] T. Cootes, D. Cooper, C. Taylor, and J. Graham, "Active shape models their training and application," *Comput. Vis. Image Understanding*, vol. 61, no. 1, pp. 38–59, 1995.

[25] S. Benameur, M. Mignotte, S. Parent, H. Labelle, W. Skalli, and J. D. Guise, "3-D/2-D registration and segmentation of scoliotic vertebrae using statistical models," *Computerized Med. Imag. Graphics*, vol. 27, no. 5, pp. 321–337, 2003.

[26] J.-M. Laferte, F. Heitz, P. Perez, and E. Fabre, "Hierarchical statistical models for the fusion of multiresolution image data," in *Proc. 5th Int. Conf. Computer Vision*, Kauai, HI, Jun. 1995, pp. 908–913.

[27] C. Kervrann and F. Heitz, "A hierarchical statistical framework for the segmentation of deformable objects in image sequences," in *Proc. IEEE Computer Society Conf. Computer Vision and Pattern Recognition*, Seattle, WA, Jun. 1994, pp. 724–728.

[28] R. Bernard, B. Likar, and F. Pernuš, "Segmenting articulated structures by hierarchical statistical modeling of shape, appearance, and topology," in *Lecture Notes in Computer Science*, M. V. E. W. J. Niessen, Ed: Springer-Verlag, 2001, vol. 2208, Proceedings of the 4th International Conference on Medical Image Computing and Computer-Assisted Intervention, pp. 499–506.

[29] J. Liu and P. Moulin, "Image denoising based on scale-space mixture modeling of wavelet coefficients," in *Proc. IEEE Int. Conf. Image Processing*, Kobe, Japan, Oct. 24–28, 1999, pp. 386–390.

[30] C. Davatzikos, X. Tao, and D. Shen, "Hierarchical active shape models, using the wavelet transform," *IEEE Trans. Med. Imag.*, vol. 22, no. 3, pp. 414–423, Mar. 2003.

[31] S. Benameur, M. Mignotte, S. Parent, H. Labelle, W. Skalli, and J. D. Guise, "A hierarchical statistical modeling approach for the unsupervised 3-D reconstruction of the scoliotic spine," in *Proc. 10th IEEE Int. Conf. Image Processing*, vol. 1, Barcelona, Spain, Sep. 2003, pp. 561–564.

[32] M. M. Panjabi, K. Takata, V. Goel, D. Frederico, T. Oxland, J. Duranceau, and M. Krag, "Thoracic human vertebrae: quantitative three-dimensional anatomy," *Spine*, vol. 16, no. 8, pp. 888–901, 1991.

[33] M. M. Panjabi, V. Goel, T. Oxland, K. Takata, J. Duranceau, M. Krag, and M. Price, "Lumbar human vertebrae: quantitative three-dimensional anatomy," *Spine*, vol. 17, no. 3, pp. 299–306, 1992.

[34] I. Semaan, W. Skalli, S. Veron, A. Templier, J. Lasseau, and F. Lavaste, "Quantitative three-dimensional anatomy of lumbar spine," *Eur. J. Orthop. Surg.*, 2001.

[35] B. Horn, "Closed-form solution of absolute orientation using unit quaternions," *J. Opt. Soc. Am.*, vol. 4, no. 4, pp. 629–642, 1987.

[36] U. Grenander and D. Keenan, "Toward automated image understanding," *J. Appl. Statist.*, vol. 16, no. 2, pp. 207–221, 1989.

[37] J. K. Canny, "A computational approach to edge detection," *IEEE Trans. Pattern Anal. Mach. Intell.*, vol. PAMI-8, no. 6, pp. 679–697, Jun. 1986.

[38] A. K. Jain, Y. Zhong, and S. Lakshmanan, "Object matching using deformable templates," *IEEE Trans. Pattern Anal. Mach. Intell.*, vol. 18, no. 3, pp. 267–278, Mar. 1996.

[39] O. François, "Global optimization with exploration/selection algorithms and simulated annealing," *Ann. Appl. Probability*, vol. 12, pp. 248–271, 2002.

[40] F. Destrempes and M. Mignotte, "Unsupervised localization of shapes using statistical models," in *Proc. Int. Conf. Signal and Image Processing, IASTED*, Kauai, HI, Aug. 2002, pp. 60–65.

[41] Z. Michalewicz, *Genetic Algorithms+Data Structures=Evolution Program*, 3nd ed. Berlin, Germany: Spring-Verlag, 1996.

[42] M. Mignotte, J. Meunier, and J.-C. Tardif, "Endocardial boundary estimation and tracking in echocardiographic images using deformable templates and markov random fields," *Pattern Anal. Applicat.*, vol. 4, no. 4, pp. 256–271, 2001.

[43] C. Pena-Reyes and M. Sipper, "Evolutionary computation in medicine: an overview," *Artif. Intell. Med.*, vol. 19, pp. 1–23, 2000.

[44] J. D. Guise and Y. Martel, "3-D-biomedical modeling: merging image processing and computer aided design," in *Proc. Int. Conf. IEEE Engineering in Medicine and Biology Society*, vol. 1, Nov. 1988, pp. 426–427.

[45] C. Aubin, J. Dansereau, F. Parent, H. Labelle, and J. D. Guise, "Morphometric evaluations of personalized 3D reconstructions and geometric models of the human spine," *Med. Biol. Eng. Comput.*, vol. 35, no. 6, pp. 611–618, 1997.

[46] S. Parent, H. Labelle, W. Skalli, B. Latimer, and J. D. Guise, "Morphometric analysis of anatomic scoliotic specimens," *Spine*, vol. 27, no. 21, pp. 2305–2311, Nov. 1, 2002.

[47] P. Borgne, W. Skalli, I. Stokes, N. Maurel, G. Beaupre, and F. Lavaste, "Three-dimensional measurement of a scoliotic spine," *Three-Dimensional Analysis of Spinal Deformities (IOS)*, pp. 219–224, 1995.

[48] D. Cox and E. Snell, *Applied Statistics: Principles and Examples*. New York: Chapman and Hall, 1982.

Said Benameur received the Diploma Engineer degree in computer engineering from the Mouloud Mammeri University, Tizi-Ouzou, Algeria, in 1990, the M.Sc. degree in computer engineering from University of Quebec at Montreal (UQAM), Montreal, QC, Canada, in 1998, and the Ph.D. degree in engineering from Engineering School (ETS), Quebec University, Montreal, QC, Canada, in 2004.

From 1993 to 1996, he was Computer Engineer at the Headquarters Civil, Algeria; He is currently a Postdoctoral Fellow in the Computer Science and Operations Research department of the University of Montreal working at the Image Processing Laboratory. His current research interests include statistical methods, deconvolution and restoration, computer vision and its applications to medical imaging.

Max Mignotte received his M.Sc. degree in(electronics and telecommunications and the DEA degree in digital signal, image and speech processing from the INPG University, Grenoble, France, in 1992 and 1993, respectively. He received the Ph.D. degree in electronics and computer engineering from the University of Bretagne Occidentale (UBO), Brittany, France, and the digital signal laboratory (GTS) of the French Naval academy, Brest, France, in 1998.

He was an INRIA Postdoctoral Fellow at the University of Montreal (DIRO), Montreal, QC, Canada, from 1998 to 1999. he was also a NSERC Postdoctoral Fellow, a Teaching Assistant and a Lecturer at the University of Montreal from September 1999 to July 2000. He is currently with DIRO at Computer Vision and Geometric Modeling Laboratory as an Assistant Professor at University of Montreal. His current research interests include statistical methods and Bayesian inference for image segmentation (with hierarchical Markovian, statistical templates, or active contour models), parameters estimation, tracking, classification, deconvolution and restoration issues in medical or sonar imagery.

Hubert Labelle received the M.D. degree and completed his residency in orthopaedics at University of Montreal, Montreal, QC, Canada,

He completed a two-year fellowship in pediatric orthopaedics at Sainte-Justine Hospital, Montreal, Rancho Los Amigos Hospital, Downey, CA, and the A.I. Du Pont Institute, Wilmington, DE.

Since 1982, he has held an appointed in the Department of Surgery at University of Montreal and at Ste-Justine Hospital where he is currently a Professor of surgery and Titular of the Motion Sciences Research Chair of Sainte-Justine Hospital and the University of Montreal. His clinical work is focused on the evaluation and treatment of scoliotic deformities in children and adolescents. He is head of the musculoskeletal research group at Sainte-Justine Hospital Research Center and Director of the Three-Dimensional Scoliosis Laboratory. His research interests include the 3–D evaluation and treatment of scoliotic deformities, with a particular emphasis on computer assisted surgery, 3-D design and evaluation of braces for the treatment of idiopathic scoliosis, and 3-D evaluation and simulation of surgery for scoliotic deformities.

Jacques A. De Guise received the B.Sc. degree in electrical engineering and his ph.d. degree in biomedical engineering from École Polytechnique of Montreal, Montreal, QC, Canada, in 1977 and 1984, respectively.

He was a Natural Sciences and Engineering Research Council (NSERC) postdoctoral scholar at the Computer Vision and Robotics Laboratory of McGill University, Montreal, QC, Canada, from 1984 to 1986. He was a NSERC Researcher Fellow at the Institut de gnie biomdical of the University of Montreal from 1986 to 1990. He is currently Full Professor at the Automated Production Department of the École de technologie supérieure of Montreal and Director of the Laboratoire de recherche en imagerie et orthopédie (LIO) of the University of Montreal Hospital Research Centre. He holds Chair of the Canada Research Chair in 3-D imaging and biomedical engineering. His current research interests are 3-D medical imaging, 3-D modeling of the musculoskeletal and vascular systems and computer assisted surgery.